# 5493 | Effects of electronic control systems on autonomous vehicle performance in granular terrain

Bohumir Jelinek [a,*], Aidan Dickerson [a], Angela Card [a], Greg Henley [a], George L. Mason [a], Ethan Salmon [a], C. Michael Gibson [a], Tyler Hannis [a], Thomas Skorupa [b], Michael Cole [b], Jody D. Priddy [c], Miriam Figueroa-Santos [b], Sara Boyle [b], Jeremy Mange [b]

[a] *Center for Advanced Vehicular Systems, Mississippi State University, Mississippi State, Mississippi, United States*

[b] *U.S. Army Combat Capabilities Development Command Ground Vehicle Systems Center, Warren, Michigan, United States*

[c] *U.S. Army Engineer Research and Development Center, Geotechnical and Structures Laboratory, Vicksburg, Mississippi, United States*

** Corresponding author: bj48@cavs.msstate.edu*

**A B S T R A C T**

Understanding the effects of electronic control systems, such as Antilock Braking System (ABS) and Electronic Stability Control (ESC), and their interaction with the steering control algorithm is critical for improving mobility and maneuverability of autonomous wheeled vehicles in off-road environments.

In this work, we evaluate the effects of wheel-speed based ABS and yaw-rate-following ESC on the performance of an autonomously-driven Polaris vehicle performing a double-lane-change (DLC) maneuver in granular terrain. The performance is evaluated in terms of the maximum speed at which the vehicle can pass the DLC test. Two lateral speed controllers are compared: a simple PID and a Stanley autonomous steering controller, along with the longitudinal speed controller that accelerates the vehicle to identify the maximum DLC passing speed. The simulations were conducted using the Chrono simulation package with the Soil Contact Model (SCM). The SCM parameters based on dry sand soil bin measurements were chosen from published literature. The ABS effects were found to be negligible or detrimental, while the ESC augmented the lateral steering control algorithm allowing the vehicle to achieve higher DLC passing speeds.

*Keywords*
Off-road mobility
Soft terrain
Electronic stability control
Antilock braking system
Double lane change

## 1. Introduction

Electronic control systems allow vehicles to better handle slippery road-surface conditions and improve the safety of occupants during emergency driving maneuvers. These systems therefore became standard for on-road vehicles. Improving vehicle mobility and driver safety for vehicles in off-road environments is less explored, presenting challenges for agriculture, construction, military, and space exploration.

This work examines the effect of Antilock Braking System (ABS) and Electronic Stability Control (ESC) on the ISO-3888-1 test performance in sand-like terrain.

## 2. Double lane change test

The double lane change test (DLC) for road vehicles is described by the ISO 3888-1 standard. The test aims to evaluate the safety of the vehicle during an aggressive lane change maneuver. The vehicle driving path during the test is constrained as shown in Fig. 1. Details for the vehicle studied in this work are shown in Fig. 4. Widths of the individual sections of the path are proportional to the width of the vehicle being tested, with the consecutive sections increasing in width. The ISO 3888-1 test targets passenger cars and light commercial vehicles with limited length, therefore the horizontal lengths of the path sections are constants not depending on the vehicle length. Lateral boundaries of sections 1, 3, and 5 are marked by cones that create boundaries for acceptable vehicle trajectories. The vehicle passes the test only if it stays within the boundaries.

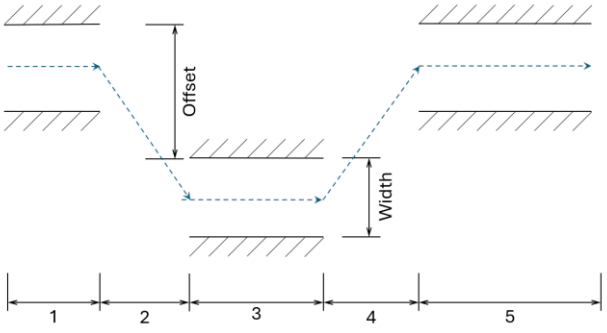


*Fig. 1 ISO-38881 double lane change maneuver*

## 3. Terrain: Soil Contact Model

The soil contact model (Krenn and Hirzinger, 2009), specifically its efficient implementation in Chrono (Serban et al., 2023), was used to model the interaction between the soil and the vehicle's wheels. The model is based on Bekker's terramechanics law

$$p = \left(\frac{K_c}{b} + K_\phi\right) z^n \tag{1}$$

(Bekker, 1956). This expression relates the normal pressure $p$ along the contact patch for a wheel with the width $b$ to the contact sinkage $z$, in terms of the coefficient $K_c$ related to soil cohesion, the coefficient $K_\phi$ related to soil stiffness, and the soil sinkage exponent $n$. The shear stress in SCM is expressed following the formulation by Janosi and Hanamoto (1961)

https://doi.org/10.56884/ABCD1234 *(ed. note: ISTVS will update your paper's DOI)*
ISBN 978-1-942112-58-7 

$$\tau = \tau_{\max}\left(1 - e^{-j/k}\right) \quad (2)$$

where $j$ is accumulated shear and $k$ is the Janosi parameter. The $\tau_{\max}$ is given by Mohr–Coulomb failure criterion

$$\tau_{max} = c + p\ tan\ (\phi) \quad (3)$$

where $c$ is the soil cohesion, where $p$ is the normal pressure from Eq. (1), and $\phi$ is the soil internal friction angle. This study applied SCM parameters for the dry sand from Guo et al. (2019) listed in Table 1.

*Table 1*
*Parameters of the SCM soil model (Guo et al., 2019)*

| Parameter | Value | Unit |
|---|---|---|
| $K_c$ | 1000 | $N/m^{n+1}$ |
| $K_\phi$ | 1528600 | $N/m^{n+2}$ |
| $n$ | 1.08 | - |
| $k$ | 0.024 | m |
| $c$ | 200 | Pa |
| $\phi$ | 27 | ° |

## 4. Chrono Polaris 3D vehicle dynamics model

The effect of control systems was studied on a 3D Polaris AWD vehicle model as implemented in the Chrono software package (Serban et al., 2019; Tasora et al., 2015). The model consists of a rigid chassis, a double wish-bone suspension in front, a three-link independent rear arm suspension in the back, and a powertrain with automatic transmission characterized by lookup tables. Most significant parameters of the vehicle model are listed in Table 2.

*Table 2*
*Parameters of the Chrono Polaris vehicle model*

| Parameter | Value | Unit |
|---|---|---|
| Mass | 1378 | kg |
| Wheelbase | 2.72 | m |
| Max steering angle | 27 | ° |
| Vehicle width | 1.51 | m |

## 5. Control systems

Four control systems were subject of this study: antilock braking system (ABS), electronic stability control (ESC), along with two steering controllers: a proportional steering controller with look-ahead and a Stanley steering controller.

### *5.1. Antilock braking system*

The ABS algorithm following the one presented in Pacejka and Besselink (2012) was applied in the present work. As described in Jelinek et al. (2024) and illustrated in Fig. 2, the ABS algorithm applied in this study examines the wheel speed, which is designated by $r_{eo}\Omega$ in the upper plot in Fig. 2, to modulate the braking effort by either 1) applying reduction gradually lowering the braking effort requested by the driver, 2) keeping the net braking effort at the constant level, or 3) increasing the braking effort gradually back to the level requested by the driver. When braking is required, the driver requests an increase in braking torque $M_B$ at the driver's desired rate up to a desired maximum value. The ABS will allow the braking torque to increase until point B is reached. After reaching point B, the torque is reduced by the ABS at a given rate $R_2$ until point C is reached, as shown in the middle plot in Fig. 2. Then, the braking torque remains constant in the interval between points C and E. At point E, when the wheel velocity has caught up sufficiently with the vehicle velocity, the braking pressure is pumped up at a rate $R_1$ until it reaches the original driver's brake request (state Z).

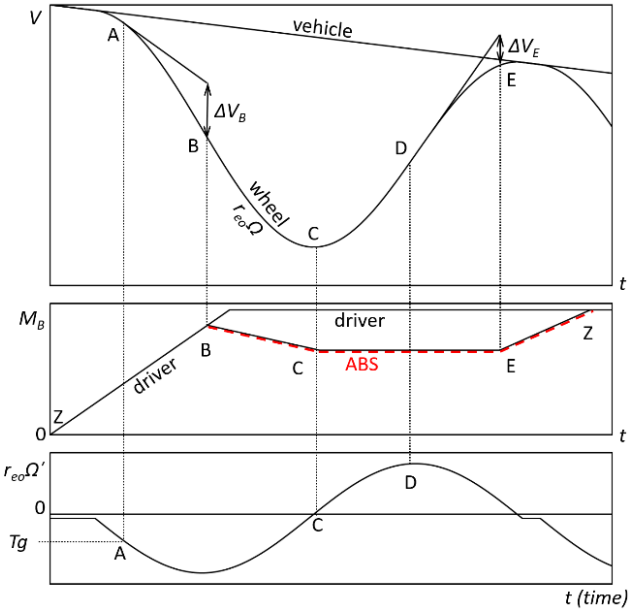


*Fig. 2 ABS algorithm*

### *5.2. Steering controllers*

Two steering controllers implemented in Chrono software suite were examined in this study.

The first steering controller was a path-following controller with look-ahead and feedback proportional to the error in projected trajectory. This path-following steering controller first constructs a cubic Bezier curve located between the DLC path boundaries as depicted by the dashed line in Fig. 4. The controller sets the steering command so that the projected path of the vehicle at the look-ahead distance (sentinel point) follows a point on the Bezier curve at the look-ahead distance (target point). For this controller, only the proportional feedback coefficient $K_P$ of the full proportional-integral-derivative (PID) version available in Chrono was tuned, while the integral and derivative feedback coefficients $K_I$ and $K_D$ were set to zero in this work to avoid the need for extensive tuning. The constant parameters of the path-following proportional steering controller and the intervals of values for the parameters varied in this study are shown in Table 3.

*Table 3*
*Parameters of path-following proportional steering controller*

| Parameter | Value / <range> | Unit |
|---|---|---|
| Look-ahead distance | 5.0 | m |
| $K_P$ | <0.1, 256> | - |
| $K_I$ | 0.0 | - |
| $K_D$ | 0.0 | - |

The second steering controller examined in this study was the Stanley path-following steering controller (Hoffmann et al., 2007). This controller was developed by a team from Stanford University for a vehicle that won the 2005 DARPA Grand Challenge (Thrun et al., 2006). It corrects both directional and lateral (cross-track) path

errors, allowing the vehicle to return to the desired path even in the presence of large disturbances. The desired steering angle $\delta$ is given by

$$\delta(t) = \psi(t) + \arctan \frac{K_S e(t)}{v(t)} \quad (4)$$

Here, the $\psi$ is the directional path error, the $e$ is the lateral (cross-track) path error, and the $v = |\boldsymbol{v}|$ is the vehicle speed as illustrated in Fig. 3. The parameter $K_S$ quantifies the corrective strength of the feedback for the lateral error.

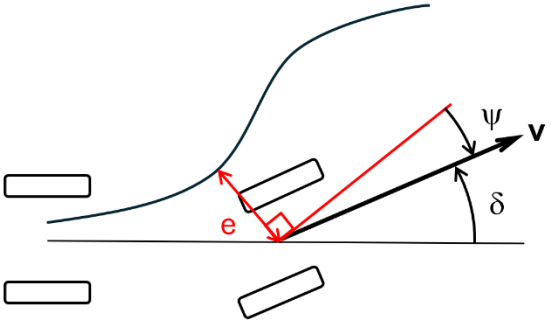


*Fig. 3 Stanley steering control variables*

The intervals of values for the parameters that were varied in this study are listed in Table 4. Additional features of the Stanley controller, as time delay, reset, dead zone, and tire dynamics, were not applied here.

*Table 4*
*Parameters of Stanley steering controller*

| Parameter | Value / <range> | Unit |
|---|---|---|
| $K_S$ | <0.1, 256> | - |

### *5.3. Electronic stability control*

The yaw-rate following ESC algorithm applies braking command correction proportional to the difference between the desired and actual yaw rate. The desired yaw rate $\omega_D$ is calculated from the steering angle $\delta$, a forward component of the vehicle velocity $v_x$ and from the vehicle wheelbase $L$ as follows.

$$\omega_D = \frac{v_x \tan(\delta)}{L} \quad (5)$$

The actual yaw rate $\omega_A$ is the angular speed of a vehicle about its vertical axis. The corrective braking command $c_F$ for the front wheels and $c_R$ for the rear wheels, both limited within the interval <0, 1> corresponding to zero braking torque and maximum braking torque, are calculated from the steering delta $\Delta = \omega_A - \omega_D$ as follows.

$$c_F = K_F \Delta, \quad c_R = K_R \Delta \quad (6)$$

The corrective braking is applied only on the left (right) side when the desired yaw rate is larger (lower) than the actual yaw rate. Yaw rate is considered positive for the left turn. The different correction coefficients $K_F$ and $K_R$ can be applied for the wheels on the front (steered) axle and the rear (not steered) axle. The ESC will activate only after $\Delta$ exceeds the threshold of 0.01 radians per second, and it will deactivate when $\Delta$ is lower than this threshold for more than one second. The ESC parameters and intervals within which the parameters were varied are listed in Table 5.

*Table 5*
*Parameters of Electronic Stability Control*

| Parameter | Value / <range> | Unit |
|---|---|---|
| Activation threshold | 0.01 | rad/s |
| Deactivation delay | 1.0 | s |
| Front correction coefficient $K_F$ | <0.01, 32> | 1/rad |
| Rear correction coefficient $K_R$ | <0.01, 32> | 1/rad |

## 6. Results

This section summarizes simulation results, showing how the controllers were tuned and assessing the effects of electronic control systems on the maximum speed at which the vehicle can pass the DLC test.

### *6.1. ABS effects on DLC test*

ABS significantly improves control of the vehicle when braking on a hard surface. The goal of the present ABS algorithm is to reduce braking effort to avoid the wheel locking (skid) and to regain the grip with the road surface. On granular terrain, represented by the SCM model in this study, the reduction of the braking command resulting from ABS action was found either negligible – when the braking was not sufficiently strong to cause excessive wheel deceleration, or detrimental – when the ABS reduction in braking interfered with the braking requested by ESC. To avoid this interference, the ABS was turned off during all ESC tests on granular terrain presented next.

### *6.2. ESC effects on DLC test without tuned steering*

Tuning of ESC parameters for the vehicle to achieve the maximum DLC-passing speed was first performed with the default values kept for the steering parameters.

The path-following proportional steering controller had the default value of $K_P = 0.5$. The DLC tests with combinations of $K_F$ and $K_R$ values of 0, 2, 4, 8, 16, 32 were executed. The vehicle passed the DLC test at the maximum speed of 10 m/s, with $K_F$:$K_R$ combinations of 4:2, 8:4, 8:2, 16:8, 16:4, 16:2 and 32:3, 32:4, 32:2. Locking of the front wheels (but not rear) when the steering delta was large was observed in each of these cases. Wheel trajectories along with target and sentinel point locations for the DLC test of the vehicle using the proportional steering controller with $K_P = 0.5$ are shown in Fig. 4. Without ESC (upper plot), the vehicle fails the DLC test due to the front right wheel leaving the course. The lower plot shows the vehicle passing the DLC test with $K_F = 4$ and $K_R = 2$. The corresponding actual and desired yaw rate, steering delta, and braking commands for the front left, front right, rear left, and rear right wheels are shown in Fig. 5.

For the Stanley steering controller with the default $K_S = 0.5$, the maximum speed for the vehicle to pass the DLC test was found to be 10 m/s. The only $K_F$:$K_R$ combination that passed the DLC test at the maximum speed 10 m/s was 32:2, which resulted in the front wheel being locked when the most intense steering was applied.

### *6.3. ESC effects on DLC test with tuned steering*

Tuning the proportional steering controller revealed that the $K_P$ values of 16 or higher resulted in the maximum DLC passing speed of 15 m/s even without ESC. When ESC was applied at 15 m/s, the $K_P$ value of 8 was sufficient with the $K_F$:$K_R$ combination of 0.01:0.01. An increased maximum DLC passing

speed of 16 m/s was then achieved with the help of ESC, but only with $K_P \geq 32$ and small $K_F$:$K_R$ combinations, as 0.02:0.02 or 0.04:0.02. The vehicle failed the test with the $K_F$:$K_R$ combinations of 0.01:0.01 and 0.04:0.04. Notably, the maximum steering angle is reached even when performing the DLC test at lower speeds. For example at 13 m/s, the minimum required $K_P = 4$ resulted in applying maximum steering angle - specifically when the vehicle turns to return to the original lane (x = 80 m in Fig. 4) and when it turns to straighten the direction of travel after returning to the original lane (x = 100 m in Fig. 4).

Tuning the Stanley steering controller led to the maximum DLC passing speed of 11 m/s - with the $K_S$ values in the interval <110, 256>. The maximum passing speed of 11 m/s was achieved without ESC, and engaging ESC did not help enough to pass the DLC test at 12 m/s.

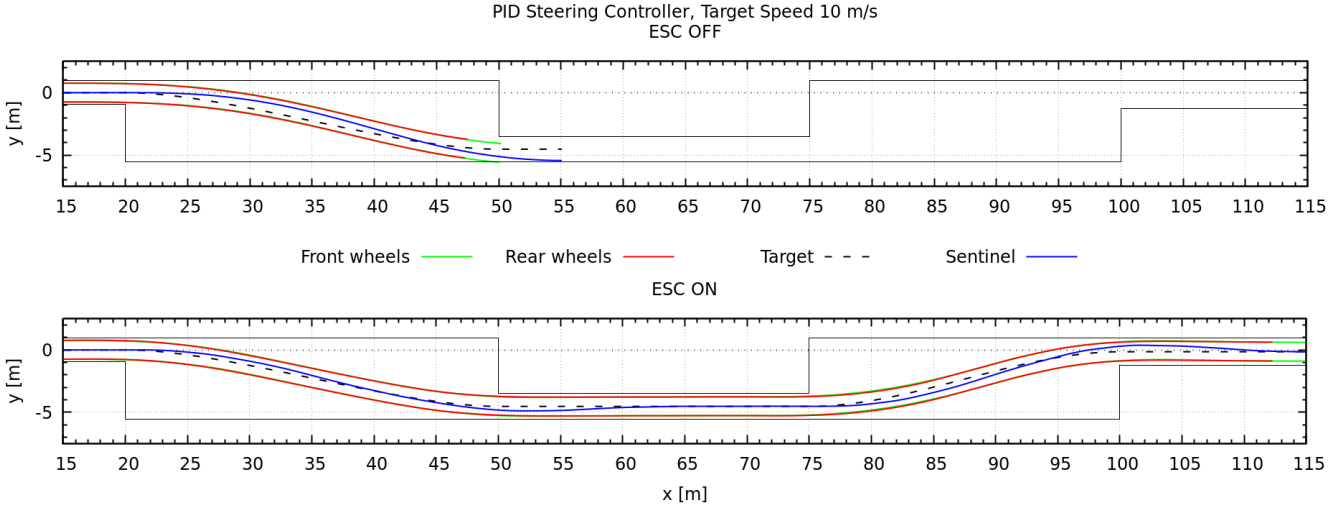


*Fig. 4 DLC with ESC versus without ESC*

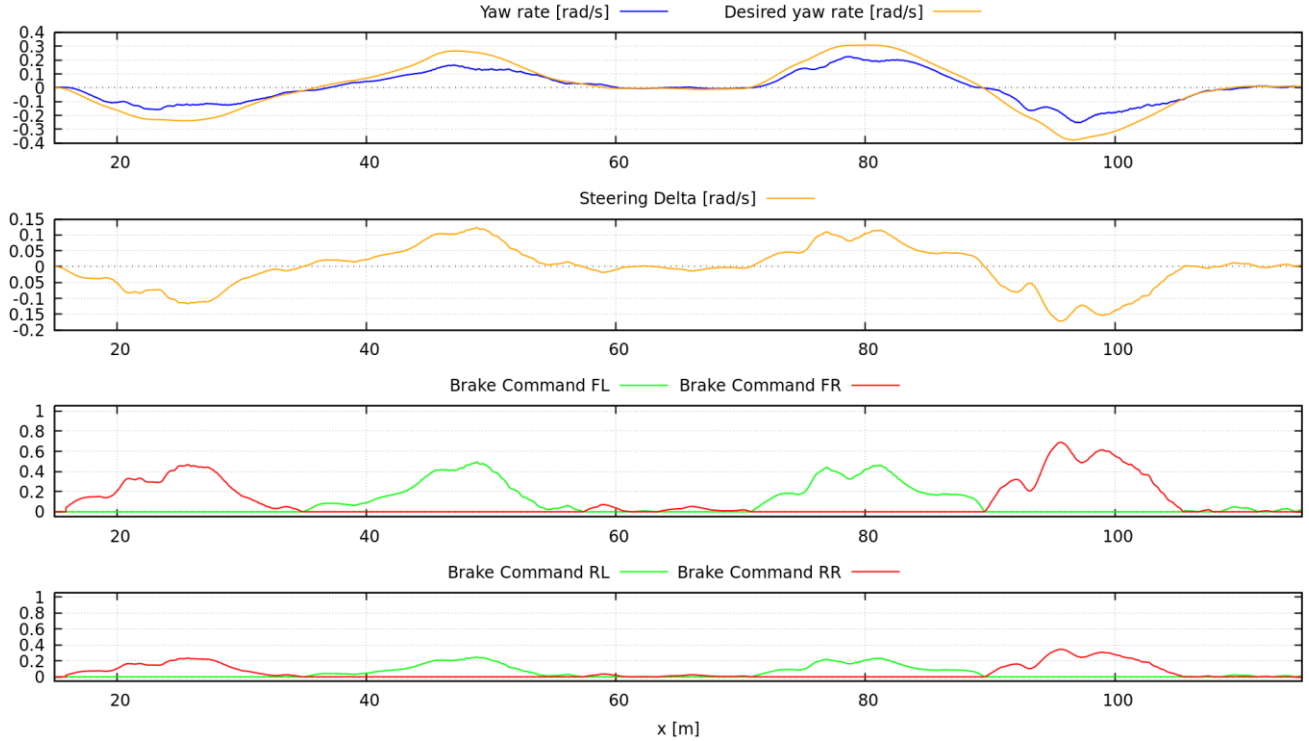


*Fig. 5 Actual and desired yaw rates, steering delta, and corrective brake commands (front left, front right, rear left, rear right) initiated by ESC*

### *6.4. Comparison of DLC tests without ESC on hard surface vs. SCM*

The maximum passing speeds and tuned parameters for the proportional and Stanley steering controller when the vehicle drives on an SCM surface and on a hard surface are listed in Table 6.

The maximum passing speed is always lower on the SCM terrain than on the hard surface. To achieve maximum DLC passing

speeds on either surface requires optimization of the steering controller's $K_P$ or $K_S$ values.

For the soft surface, it proved more difficult to find a single optimal value than for the hard surface. Numerous runs for the Stanley controller were examined to identify the range of parameters where the vehicle passed the test. Just outside the boundaries of this range, some of the tests have failed and some passed. Further from the boundaries, all tests failed.

With the Stanley controller, the optimal $K_S$ for soft surface is much larger than for the hard surface.

*Table 6*
*Max passing speed without and with ESC on SCM surface vs. hard surface*

| Steering controller | Hard surface | | SCM surface | | |
|---|---|---|---|---|---|
| | Tuned parameter | Max DLC passing speed | Tuned parameter | Max DLC passing speed | With ESC |
| Proportional | $K_P$ =20 | 24 m/s | 11≤$K_P$≤64 | 15 m/s | 16 m/s |
| Stanley | $K_S$ =0.2 | 19 m/s | 110≤$K_S$≤430 | 11 m/s | 11 m/s |

## 7. Conclusions and future work

The present study revealed that only minimal ESC intervention was required when the proportional steering feedback coefficient $K_P$ was tuned to achieve the highest DLC speed on the sand-like SCM surface. However, the ESC helped to increase the maximum DLC passing speed when the steering was not tuned, compensating for the low value of the steering feedback coefficient $K_P$. With the Stanley steering controller, ESC did not help to improve maximum DLC passing speed.

The proportional path-following steering controller allowed the vehicle to pass the DLC test at significantly higher speeds than the Stanley steering controller, demonstrating that robustness of Stanley controller comes with a cost of accuracy in the case of a tight-boundary DLC test on a homogeneous SCM surface. With increased speed, the two steering controllers required higher values of $K_P$ and $K_S$, respectively.

For future work, the effects of the look-ahead distance parameter should be studied. The derivative and integral feedback should also be evaluated for improvement of the steering stability. Other steering controllers, for example simple-realistic and pure-pursuit controllers, need to be examined and a wider range of testing scenarios should be deployed. Given that the maximum steering angle was reached in many of the SCM tests, simulations with increased maximum steering angle could be performed to check for increased maximum DLC passing speed.

## 8. Acknowledgements

This material is based upon research conducted under contract W912HZ-22-C0004 with the U.S. Army Engineer Research and Development Center (ERDC). The views and conclusions contained herein are those of the authors and should not be interpreted as necessarily representing the official policies or endorsements, either expressed or implied, of ERDC or the U.S. Government.

## 9. Declaration of competing interest

The authors declare that they have no known competing financial interests or personal relationships that could have appeared to influence the work reported in this paper.

## 10. References

Bekker, M.G., 1956. Theory of Land Locomotion: The Mechanics of Vehicle Mobility, 9690401st ed. University of Michigan Press, Ann Arbor, MI. https://doi.org/10.3998/mpub.9690401

Guo, T., Guo, J., Huang, B., Peng, H., 2019. Power consumption of tracked and wheeled small mobile robots on deformable terrains–model and experimental validation. Mech. Mach. Theory 133, 347–364. https://doi.org/10.1016/j.mechmachtheory.2018.12.001

Hoffmann, G.M., Tomlin, C.J., Montemerlo, M., Thrun, S., 2007. Autonomous Automobile Trajectory Tracking for Off-Road Driving: Controller Design, Experimental Validation and Racing. IEEE, pp. 2296–2301. https://doi.org/10.1109/ACC.2007.4282788

Janosi, Z., Hanamoto, B., 1961. The analytical determination of drawbar pull as a function of slip for tracked vehicles in deformable soils, in: International Society for Terrain-Vehicle Systems, 1st Int. Conf.

Jelinek, B., Henley, G., Card, A., Hannis, T., Gibson, M., Priddy, J., Boyle, S., Figueroa-Santos, M., Mange, J., 2024. Vehicle-Level Control Systems Framework for Use in Create-GV Vehicle Dynamics Simulations. Presented at the 2024 NDIA Michigan Chapter Ground Vehicle Systems Engineering and Technology Symposium, Novi, Michigan, United States, pp. 2024-01–4107. https://doi.org/10.4271/2024-01-4107

Krenn, R., Hirzinger, G., 2009. SCM – A SOIL CONTACT MODEL FOR MULTI-BODY SYSTEM SIMULATIONS, in: Proceedings of the 11th European Regional Conference of the ISTVS.

Pacejka, H.B., Besselink, I., 2012. Tire and vehicle dynamics, 3rd edition. ed. Butterworth-Heinemann Elsevier, Oxford Waltham.

Serban, R., Taves, J., Zhou, Z., 2023. Real-Time Simulation of Ground Vehicles on Deformable Terrain. J. Comput. Nonlinear Dyn. 18. https://doi.org/10.1115/1.4056851

Serban, R., Taylor, M., Negrut, D., Tasora, A., 2019. Chrono::Vehicle: template-based ground vehicle modelling and simulation. Int. J. Veh. Perform. 5, 18. https://doi.org/10.1504/IJVP.2019.097096

Tasora, A., Serban, R., Mazhar, H., Pazouki, A., Melanz, D., Fleischmann, J., Taylor, M., Sugiyama, H., Negrut, D., 2015. Chrono: An open source multi-physics dynamics engine, in: Kozubek, T. (Ed.), International Conference on High Performance Computing in Science and Engineering, Lecture Notes in Computer Science. Springer, pp. 19–49.

Thrun, S., Montemerlo, M., Dahlkamp, H., Stavens, D., Aron, A., Diebel, J., Fong, P., Gale, J., Halpenny, M., Hoffmann, G., Lau, K., Oakley, C., Palatucci, M., Pratt, V., Stang, P., Strohband, S., Dupont, C., Jendrossek, L., Koelen, C., Markey, C., Rummel, C., van Niekerk, J., Jensen, E., Alessandrini, P., Bradski, G., Davies, B., Ettinger, S., Kaehler, A., Nefian, A., Mahoney, P., 2006. Stanley: The robot that won the DARPA Grand Challenge. J. Field Robot. 23, 661–692. https://doi.org/10.1002/rob.20147